JACS
JOURNAL OF THE AMERICAN CHEMICAL SOCIETY
Article
pubs.acs.org/JACS

A Mechano-Electronic DNA Switch

Jason M. Thomas,[†,‡] Hua-Zhong Yu,*[,‡] and Dipankar Sen*[,†,‡]

[‡]Department of Chemistry and [†]Department of Molecular Biology and Biochemistry, Simon Fraser University, Burnaby, British Columbia, Canada V5A 1S6

Supporting Information

ABSTRACT: We report a new kind of DNA nanomachine that, fueled by Hg^{2+} binding and sequestration, couples mechanical motion to the multiply reversible switching of through-DNA charge transport. This mechano-electronic DNA switch consists of a three-way helical junction, one arm of which is a T-T mismatch containing Hg^{2+}-binding domain. We demonstrate, using chemical footprinting and by monitoring charge-flow-dependent guanine oxidation, that the formation of T-Hg^{2+}-T base pairs in the Hg^{2+}-binding domain sharply increases electron−hole transport between the other two Watson−Crick-paired stems, across the three-way junction. FRET measurements are then used to demonstrate that Hg^{2+} binding/dissociation, and the concomitant increase/decrease of hole transport efficiency, are strongly linked to specific mechanical movements of the two conductive helical stems. The increase in hole transport efficiency upon Hg^{2+} binding is tightly coupled to the movement of the conductive stems from a bent arrangement toward a more linear one, in which coaxial stacking is facilitated. This switch offers a paradigm wherein the performance of purely mechanical work by a nanodevice can be conveniently monitored by electronic measurement.

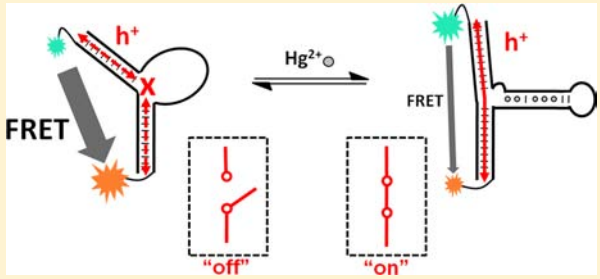

INTRODUCTION

The use of DNA to produce stimuli-responsive mechanical devices on the nanoscale ("molecular machines") has attracted much attention in recent years.[1] Ideally, these nanomachines perform a reversible and repeatable mechanical motion, powered by cycles of chemical reactions or interactions with a molecular fuel of some sort. DNA is particularly attractive for such applications in that its primary sequence directly and predictably encodes the ability to form and/or switch between topologically distinct secondary structures in response to chemical stimuli. Because of the general rigidity of DNA's secondary structure elements, such structure switching can translate into discrete, nanoscale molecular motions that could potentially be harnessed to power nanoscale mechanical devices or provide a physical response in analytical sensors. For example, pH-responsive (H^+-fueled) mechanical switching has been achieved on the basis of reversible triplex[2] or i-motif[3] formation. DNA quadruplex formation, fueled by potassium ion (K^+) binding, has also been exploited to elicit mechanical motion in DNA constructs,[4] as has a B-DNA to Z-DNA structural transition promoted by $Co(NH_3)_6^{3+}$ addition.[5] Although a stimulus of greater chemical complexity, oligonucleotide binding/sequestration has been used to program the motion of rather complex DNA machines that accomplish precisely controlled nanoscale structural rearrangements.[6,7] Prototypical "DNA walkers" have also been described powered by oligonucleotide addition/sequestration cycles,[8] by DNAzyme-catalyzed cleavage of RNA substrates,[9] or even by photolysis reactions.[10]

Conformational switching of DNA helical junctions in response to chemical stimuli has been an attractive idea for the design of nanoswitching devices. In terms of mechanical switching, reversible reorientation of the helical arms of a four-way junction has been observed in response to oligonucleotide binding/sequestration.[11] Three-way junctions, however, represent an even more promising structure-switching motif. One strategy has involved attachment of an aptamer domain as one of the three arms that form the junction, where conformational change in the aptamer upon binding to its target induces reorientation of the junction arms relative to one another.[12,13] Such aptamer-containing DNA three-way junctions have found success in the design of analytical sensors for a wide variety of analytes (*vide infra*).[12] The purely mechanical movement of such junctions, in the absence of monitoring of electronic properties, has also been reported in a separate study.[13] However, in none of the above cases was *reversibility* of switching, especially over multiple cycles, either sought or demonstrated.[12,13]

The intrinsic electron−hole (h^+) transport properties imparted by nucleobase stacking have spurred interest in exploiting DNA structure-switching to create nanoscale electronic devices/components. Therein, presumed mechanical distortion of the switch DNA, and accompanying changes in base stacking arrangements, led to a net change in its hole transport efficiency. Such DNA charge transport switching at three-way junctions has shown promise as the functional basis

Received: April 25, 2012
Published: July 26, 2012

dx.doi.org/10.1021/ja303530y | J. Am. Chem. Soc. 2012, 134, 13738−13748

for aptamer-based analytical sensors that provide an electrical signal output (so-called "deoxyribosensors").[12] In this case, charge transport through a three-way junction placed between two conductive duplex DNA stems is regulated by conformational changes in an aptamer domain, which forms the third arm of the junction. Analyte-binding-induced conformational change in the aptamer domain presumably enhances coaxial stacking and thus electrical contact between duplex domains so that charge can flow between them. When redox labeled deoxyribosensors are attached to gold electrodes, analyte-binding-induced charge transport switching produces a sensitive analytical readout in the form of an increased voltammetric signal. In another example of DNA charge transport switching, the reversible formation of conductive G-quadruplexes serves as the functional basis for charge transport switching between two duplex DNA domains that flank the quadruplex-forming domain.[14] However, in all of these systems, direct evidence for a presumed mechanical basis for the observed ligand-mediated enhancement of charge transport has not been obtained to date.

As reviewed above, mechanical[13] and electronic[12] switching have been separately demonstrated in a few three-way junction-based DNA nanomachines. However, (a) the *causal* connection between mechanical and electronic switching has not been demonstrated unequivocally in these cases, and (b) the reversibility of switching has neither been sought nor demonstrated.

In this study, we have created a three-way junction-based DNA machine which exhibits fully, and multiply, reversible, concomitant mechanical and electrical switching in response to simple chemical stimuli. Structural switching is fueled by the binding of mercuric cations (Hg^{2+}) to T-T mismatches present in one of the three-way junction stems and can be readily reversed by sequestration of Hg^{2+} by dithiothreitol (DTT). Hg^{2+} is well-known for its formation of highly specific "sandwich" complexes at T-T mismatch sites in DNA, in which a Hg^{2+} is bonded linearly between the N1 nitrogens of thymine residues on either side (T-Hg^{2+}-T).[15] It is worth pointing out that formation of this highly specific interaction represents a chemically orthogonal fuel to those used in other DNA nanomachines (for example: H^+, K^+, $Co(NH_3)_6^{3+}$, or oligonucleotides). Indeed, the unique metal cation specificity of T-Hg^{2+}-T base pair formation has been exploited by numerous investigators to generate mercury sensors of varying sensitivity and practical utility[16] but has not, to our knowledge, been used to fuel the action of DNA-based electronic devices or nanomachines.

Here, we use a chemical assay to show that through-DNA electron–hole transport across the three-way junction interface increases sharply in response to Hg^{2+} addition. We then use fluorescence (Förster) resonance energy transfer (FRET) to demonstrate that these DNA three-way junction electronic switches are also *bona fide* machines, with their 'open' (T-T mismatched) and 'closed' (Hg^{2+}-bound) conformers showing markedly distinct conformations. Quantitative comparisons between these two Hg^{2+}-dependent responses suggests that the hole transport switching correlates closely with a mechanical switching action, in which the two conductive DNA stems move further apart from each other and realign toward a coaxially stacked arrangement.

MATERIALS AND METHODS

General. Unmodified and 5′-C6-NH_2-, 5′- Cy3-, and 5′-Cy5-modified oligonucleotides were synthesized by Integrated DNA Technologies. Unmodified oligonucleotides were purified by denaturing PAGE (7 M Urea/TBE), eluted by crush and soak into 10 mM Tris-HCl (pH 8.0), ethanol precipitated, and desalted using improvised G-25 spin columns (G-25 from Sigma). 5′-anthraquinone-conjugated oligonucleotide C1 (AQ-C1) was prepared by reaction of 5′-C6-NH_2-modified oligonucleotide C1 with the *N*-hydroxysuccinimidyl-ester of anthraquinone-2-carboxylic acid[17] as described previously.[12] Anthraquinone-, Cy3-, and Cy5-conjugated oligonucleotides were purified by HPLC: 250 × 4.6 mm Gemini 5 μm-C18 column (Phenomenex); solvent A: 0.1 M triethylammonium acetate (pH 7.0)/CH_3CN (20:1) and solvent B: CH_3CN; 20 min linear gradient from 5% solvent B to 30% solvent B; flow rate of 1.0 mL/min. For samples containing anthraquinone-, Cy3-, and Cy5-conjugated oligonucleotides, exposure to ambient light was limited as much as possible. Oligonucleotides were 5′-^{32}P-labeled using T4 polynucleotide kinase (Invitrogen) and γ-^{32}P-ATP (Perkin-Elmer) following the manufacturer's instructions, and PAGE purified as described above. Labeled oligonucleotides were ethanol precipitated following the labeling reaction, resuspended in 10% aqueous piperidine, heated at 90 °C for 30 min; this treatment cleaves any pre-existing DNA lesions that might interfere with downstream experiments that involve the analysis of DNA damage by piperidine cleavage analysis. Following piperidine treatment, the ^{32}P-labeled oligonucleotides were lyophilized extensively, PAGE-purified, and desalted as described above. Autoradiography imaging and quantification of gels were performed using a Typhoon 9410 phosphorimager with ImageQuant v5.2 software. Quantitative data were plotted and fitted using Sigma Plot v10. The aqueous $Hg(OAc)_2$ stock solutions and serial dilutions thereof were prepared freshly for each experiment as precipitation was observed on storage.

Oligonucleotide Sequences.

C1: 5′-$H_2N(CH_2)_6OPO_3$-TTT AGC TCA CGA GAC GCT CCC ATA GTG A-3′
C1: 5′-$H_2N(CH_2)_6OPO_3$-TTT AGC TCA CGA GAC GCT CCC ATA GTG A-3′
AQ-C1: C1-oligoucleotide 5′-labeled with anthraquinone (via C6-linker)
Cy3-C1: C1-oligonucleotide 5′-labeled with Cy3 (via C6-linker)
C2: 5′-TCA CTA TGG GAG CGT CTC GTG AGC TAA A
Cy5-C2: C2-oligonucleotide 5′-labeled with Cy5 (via C6-linker)
3′AA-1: 5′-TCA CTA TGG GAG CGT TTG TTT GCG GGA GCT TTC TTA AAT CTC GTG AGC TAA A-3′
Cy5–3′AA-1: 3′AA-1 oligonucleotide labeled with Cy5 (via C6-linker)
3′AA-2: 5′-TCA CTA TGG GAG CGT TTT GTT TGC GGG AGC TTT CTT AAA ATC TCG TGA GCT AAA-3′
3′CC-1: 5′-TCA CTA TGG GAG CGT TTT GTC GGG AGA CTT TTC CTC TCG TGA GCT AAA-3′
3′CC-2: 5′-TCA CTA TGG GAG CGC TTT TGT CGG GAG ACT TTT GCC TCT CGT GAG CTA AA-3′
5′CC-1: 5′-TCA CTA TGG GAG CGC CTT TTG TCG GGA GAC TTT TTC TCG TGA GCT AAA-3′
5′CC-2: 5′-TCA CTA TGG GAG CGC CGT TTT GTC GGG AGA CTT TTC TCT CGT GAG CTA AA-3′
NB-1: 5′-TCA CTA TGG GAG CGT TTT GTC GGG AGA CTT TTT CTC GTG AGC TAA A-3′
NB-2: 5′-TCA CTA TGG GAG CGC TTT TGT CGG GAG ACT TTT GTC TCG TGA GCT AAA-3′

DNA Charge Transport Experiments. Three-way junction and duplex constructs were annealed by heating the 5′-anthraquinone-labeled oligonucleotide (AQ-C1) and the 5′-^{32}P-labeled Hg^{2+}-binding switch oligonucleotide to 95 °C for 2 min in 10 mM Tris-HCl (pH 8.0), followed by slow cooling to room temperature over the course of ∼1 h. At this point, binding buffer (5 mM $MgCl_2$, 50 mM Tris-HCl,

pH 8.0) was added, followed by the desired amount of $Hg(OAc)_2$. The final concentrations of the DNA strands were 100 nM for AQ-C1 and 80 nM Hg^{2+}-binding switch oligonucleotide. Samples were then transferred to a polystyrene 96-well ELISA plate which was equilibrated in contact with a water bath at 4 °C. Irradiation was carried out inside a cold room (4 °C) by placing the ELISA plate 4 cm below a UVP Black-Ray UVL56 lamp (365 nm) for 30 min. To ensure uniform irradiation, samples were loaded into only the two rows of ELISA plate wells that were positioned directly underneath and equidistant from the UV lamp. Following irradiation, the samples were transferred to microcentrifuge tubes and ethanol precipitated. The pelleted DNA was resuspended in 100 μL of 10% aqueous piperidine (v/v), heated to 90 °C for 30 min, and then lyophilized extensively. The products were analyzed by 15% denaturing PAGE. The extent of oxidative damage to the reporter guanines was measured as the combined intensity of the G_8 and G_9 cleavage bands divided by the total intensity of all bands in the lane (i.e., the fraction of labeled oligonucleotide cleaved at G_8 and G_9). The $[Hg^{2+}]$ dependence of reporter guanine damage was analyzed by plotting $\Delta I/I_0$ (the change in $G_8 + G_9$ cleavage at a given Hg^{2+} concentration (ΔI) divided by the fraction of $G_8 + G_9$ cleavage observed in the absence of Hg^{2+} (I_0)). These data were fitted to a cooperative binding isotherm:

$$(\Delta I/I_0) = (\Delta I/I_0)_{\text{initial}} + \frac{(\Delta I/I_0)_{\max}[Hg^{2+}]^n}{K_d + [Hg^{2+}]^n} \quad (1)$$

Chemical Footprinting/Sequencing Experiments. Three-way junction constructs were annealed as described above, with the exception that oligonucleotide C1 was not conjugated to anthraquinone, although the C6-amino modification was present. Thymine-specific cleavage reactions were conducted by adding 2.5 μL of 20% pyridine followed by 2.5 μL aqueous 20 mM OsO_4 to each annealed 45 μL reaction aliquot (with either 0 μM or 10 μM Hg^{2+}). Reactions were continued for 5 min on ice, terminated by the addition of 2 μL of allyl alcohol, and ethanol precipitated. G-specific cleavage reactions were conducted in 10 mM Tris-HCl (pH 8.0)/0.1 mM EDTA by adding 1/10th volume of 10% dimethylsulfate in ethanol. Reactions were continued for 2 min on ice, terminated by the addition of 2 μL of β-mercaptoethanol, and ethanol precipitated. All chemical modification samples were treated with 10% piperidine for 30 min at 90 °C and lyophilized extensively. Reaction products were resolved by 12% denaturing PAGE.

FRET Experiments. Fluorophore-labeled oligonucleotides were annealed as described above in 10 mM Tris-HCl with oligonucleotide concentrations of 10 μM each. Samples were made up to 10% glycerol and loaded onto 10% native PAGE gels (40 mM Tris-borate buffer) run at 4 °C. 3′AA-1 and duplex complexes were well resolved from single stranded oligonucleotides, and the appropriate bands were excised from the gel and eluted by crush and soak (overnight at 4 °C) into ∼10 gel volumes of 40 mM Tris-borate. Gel purified complexes were maintained at 4 °C during storage and all manipulations. Eluted sample concentrations were determined by UV−vis absorption measurement at 260 nm. All samples for FRET experiments contained: 80 nM purified complex (3′AA-1 or duplex), 50 mM Tris-HCl (pH 8), 5 mM $MgCl_2$, 8 mM Tris-borate, and 1 mg/mL glycogen. Hg^{2+} was titrated into the samples by adding small aliquots (<0.1% by volume) of concentrated $Hg(OAc)_2$ solutions. Significant nonspecific binding of DNA to the quartz fluorescence cuvette was observed in early experiments carried out in the absence of glycogen. This effect was suppressed by incubating binding buffer containing 1 mg/mL glycogen in the clean cuvette for 1 h prior to experiments and inclusion of glycogen in the experimental samples (as above).

Steady state fluorescence emission spectra were recorded at 4 °C on a Fluoromax 3 fluorimeter (Horiba/Jobin Yvon). Polarization artifacts were minimized by setting the polarizers to "magic angle conditions" (excitation polarizer: 0°, emission polarizer: 54.7°). Spectra were acquired twice and averaged. Spectra were corrected for lamp intensity, background spectra were subtracted, and an instrument-specific correction was applied ("MCORRECT"). FRET efficiencies were calculated using the $(\text{ratio})_A$ method, which has been described in detail previously.[18] The work of Lu and co-workers, who studied Cy3/Cy5 labeled 8-17 DNAzyme folding,[19] was particularly relevant to the present study. Briefly, the quantity $(\text{ratio})_A$ is the ratio of acceptor emission intensity due to FRET (upon donor excitation at λ_{ex}^D = 513 nm) to acceptor emission intensity upon direct excitation of the acceptor at λ_{ex}^A = 648 nm. Because the donor and acceptor emission spectra overlap, the former must be subtracted from the FRET spectrum to obtain the acceptor emission intensity due to FRET (see Supporting Information). The value of $(\text{ratio})_A$ is thus calculated according to:

$$(\text{ratio})_A = \frac{F^{AD}(\lambda_{em}, \lambda_{ex}^D) - \alpha F^D(\lambda_{em}, \lambda_{ex}^D)}{F^{AD}(\lambda_{em}, \lambda_{ex}^A)} = \frac{\varepsilon^A(\lambda_{ex}^D)}{\varepsilon^A(\lambda_{ex}^A)} + d^+ E_{FRET}\frac{\varepsilon^D(\lambda_{ex}^D)}{\varepsilon^A(\lambda_{ex}^A)} \quad (2)$$

where $F^{AD}(\lambda_{em}\lambda_{ex}^D)$ is the emission intensity of the dual labeled complex at the donor excitation wavelength, $F^D(\lambda_{em}\lambda_{ex}^D)$ is the emission intensity of the donor-only labeled complex, $F^{AD}(\lambda_{em}\lambda_{ex}^A)$, and α is a weighting factor obtained by fitting the donor-only spectrum to the FRET spectrum over the wavelength range where the acceptor does not emit (525−600 nm). The FRET efficiency (E_{FRET}) can then be calculated once the necessary extinction coefficient ratios have been determined from absorption spectra. For HPLC purified samples, as used in this study, the fraction of DNAs labeled with the Cy3 donor (d^+) is taken as 100%. The $[Hg^{2+}]$ dependence of the E_{FRET} data was fit to:

$$E_{FRET} = E_{FRET}^0 + \frac{\Delta E_{FRET}^{\max}[Hg^{2+}]^n}{K_d + [Hg^{2+}]^n} \quad (3)$$

where E_{FRET}^0) is the FRET efficiency in the absence of Hg^{2+}, $\Delta E_{FRET}^{\max}$ is the maximal change in FRET efficiency at saturating $[Hg^{2+}]$, K_d is the apparent Hg^{2+} dissociation constant, and n is a Hill coefficient. Average distances (R) between FRET donor and acceptor were estimated from E_{FRET} values based on the relationship:

$$E_{FRET} = \frac{R_0^6}{R_0^6 + R^6} \quad (4)$$

where R_0 is the donor−acceptor separation at which the FRET efficiency is half maximal. R_0 is related to the value of an orientation factor, κ, which describes the directional orientation of the fluorophore transition dipole moments.[18] Here, we use C6-linked Cy3 and Cy5, attached to the 5′-end of DNA oligonucleotides. Studies by Lilley and co-workers had suggested that the use of short linker lengths (C3) to attach cyanine fluorophores to the 5′ ends of DNA led to the stacking of the dyes upon the blunt ends of DNA helices to some extent, limiting the rotational freedom of the fluorophores,[20] which in turn affects the value of κ and R_0.[21] However, C6-linked Cy3/Cy5 FRET pairs have been used with great success in prior studies to study folding transitions in nucleic acids.[19] For our purposes of estimating the change in distance between the Cy3- and Cy5-labeled helical termini, we make the simplifying assumption that the fluorophores can freely rotate, in which case $\kappa = 2/3$. On the basis of this assumption, a value of 60 Å for R_0 (from reference 21) leads to a reasonable average distance estimate, at least in the case of the duplex control.

RESULTS AND DISCUSSION

DNA Nanoswitch Design. Our three-way junction DNA electronic switch design is based on the hypothesis that formation of coaxial stacking interactions at the junction between two conductive helical stems creates electrical contact, such that charge can flow between them. Prior studies on DNA three-way junctions involving three Watson−Crick-paired stems have shown that they are able to adopt conformations in which two of the three stems adopt a nearly linear coaxial arrangement, as long as there are two or more unpaired

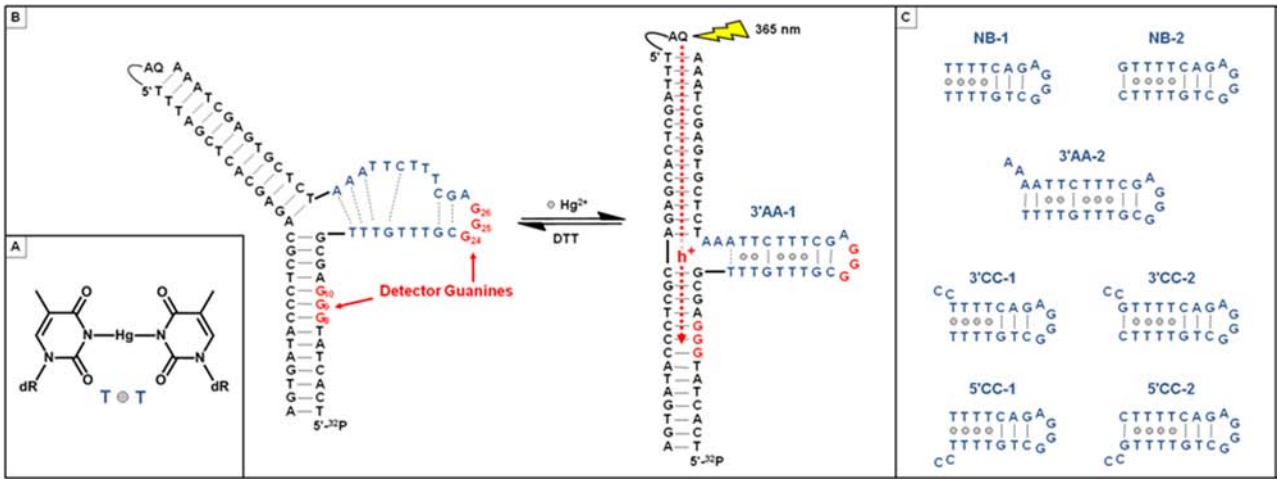

Figure 1. (A) Structure of a Hg^{2+}-mediated T-T base pair. (B) Secondary structure representations of the 3′AA-1 Hg^{2+}-driven mechano-electronic switch examined in detail in this study. Sequences in black are hole-conducting helical stems; sequences in blue are the Hg^{2+}-binding domain. The detector guanines (red) suffer oxidative damage as a result of through-DNA hole transport from photoexcited anthraquinone (AQ) through the conductive stems and three-way junction. (C) The other seven Hg^{2+}-binding domains initially examined. In all cases, the hole-conducting sequences were the same as shown in panel (B). The construct names reflect the position (at the 5′- or 3′-end of the Hg^{2+}-binding domain) and sequence (AA or CC) of the two bulged nucleotides at the three-way junction. NB denotes no bulged nucleotides.

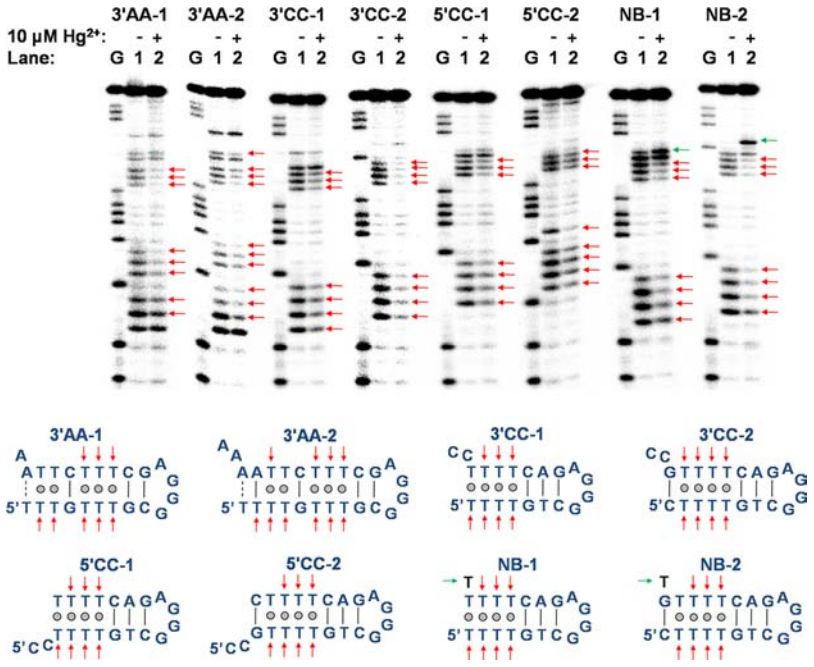

Figure 2. OsO_4 footprinting analysis of Hg^{2+}-dependent folding of the three-way junction constructs shown in Figure 1. (5′-^{32}P-labeled Hg^{2+}-binding strand). Lane 1: 3′AA-1 G-specific cleavage sequencing ladder; lane 2: thymine specific reactivity of 3′AA-1 with OsO_4 in the absence of Hg^{2+}; lane 3: thymine specific reactivity of 3′AA-1 with OsO_4 in the presence of 10 μM Hg^{2+}. OsO_4 reactivity protection upon Hg^{2+} binding is indicated by red arrows, and reactivity enhancements are indicated by green arrows. These data are mapped onto the Hg^{2+}-binding domain secondary structures below (note that the conductive stems were present, but for brevity, only the Hg^{2+}-binding domains are shown).

additional nucleotides at the junction. The specifics of the position and sequence of the unpaired nucleotides at the junction are also relevant.[22,23] On the basis of these earlier reports, we reasoned that it might be possible to design junctions, across which charge transport efficiency could toggle between 'off'- and 'on'-states by virtue of the third arm at the junction changing its structure—being relatively unstructured and base-paired in the 'off' and 'on' states, respectively. The binding of Hg^{2+} to T-T mismatches to form unnatural T-Hg^{2+}-T base-pairs could provide a straightforward and robust means for initiating such switching between the desired unstructured and base-paired forms.

We designed and tested eight potential Hg^{2+}-responsive DNA switches consisting of DNA three-way junctions made up of two conductive Watson−Crick-paired stems along with a hairpin loop containing T-T mismatches near the junction (Figure 1). In all of the cases shown in Figure 1, this mismatched hairpin loop is predicted to form a structured, helical stem upon the formation of T-Hg^{2+}-T base pairs. The effects of incorporating two bulged cytidine residues at either the 5′- or 3′- attachment point of the Hg^{2+}-binding stem was

dx.doi.org/10.1021/ja303530y | J. Am. Chem. Soc. 2012, 134, 13738−13748

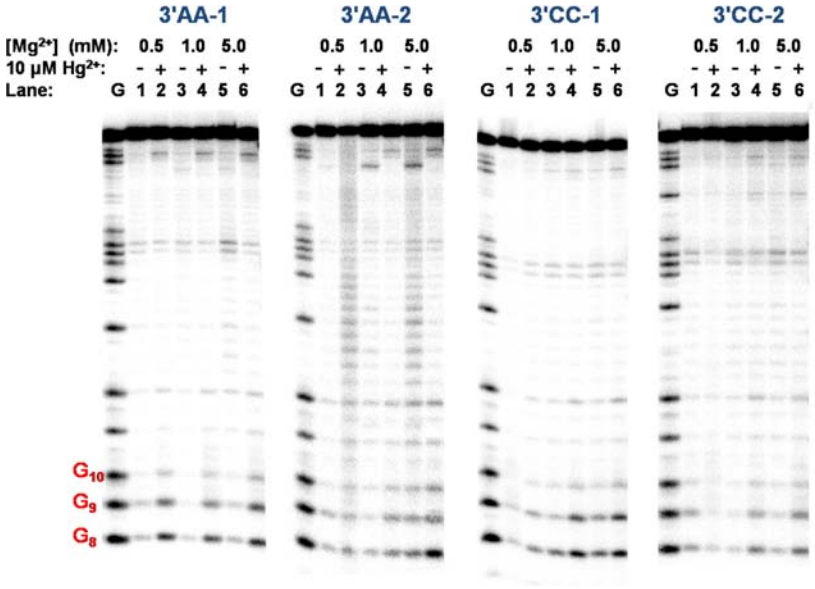

Figure 3. Survey of charge-flow-generated guanine damage patterns of different three-way junction switch constructs assembled using the Hg^{2+}-binding domains shown in Figure 1B and 1C. Charge flow was assayed in the absence (-) and presence (+) of 10 μM Hg^{2+}, at three different Mg^{2+} concentrations (0.5, 1.0, and 5.0 mM). From left to right data are shown for 3′AA-1, 3′AA-2, 3′CC-1, and 3′CC-2. Guanine triplets of interest (G_8-G_{10} and G_{24}-G_{26}) that are indicators of oxidative damage are marked in red in correspondence to Figure 1.

tested in constructs 5′CC-1, 5′CC-2, 3′CC-1, and 3′CC-2. In two cases (3′AA-1 and 3′AA-2), the sequence of the bulged nucleotides (two adenosines) was chosen such that an alternate base pairing scheme (dotted lines in Figure 1B) might be possible near the junction in the absence of T-Hg^{2+}-T base pair formation. We reasoned that structural switching might be accentuated by such alternate base pairing in the 'off'-state, which could encourage a distinctly different junction structure reminiscent of a three-way junction lacking bulged nucleotides (interhelical stacking at such junctions is strongly disfavored,[22] and would be expected to effectively prevent charge transport across the junction in the 'off'-state). For comparison, two constructs that lack bulged nucleotides at the junction in the Hg^{2+}-bound state were also examined (NB-1 and NB-2). Finally, we also compared the effects of the presence of a T-Hg^{2+}-T vs a natural base pair immediately adjacent to the junction (constructs numbered 1 vs 2, respectively).

Hg^{2+}-Binding Visualized by Chemical Footprinting. First, we sought to visualize Hg^{2+} binding to the DNA three-way junction variants, and confirm that it induces helical stem formation within the Hg^{2+}-binding domains. We therefore carried out OsO_4 reactivity protection assays, in which relative susceptibility to damage by reaction with OsO_4 is taken as a measure of the degree to which a given thymine base is protected from bulk solution by nucleobase stacking interactions.[22] The extent of reaction of specific thymine residues with OsO_4 is revealed by the extent of hot piperidine-mediated cleavage of the DNA backbone at such sites.

The OsO_4 reactivity patterns (Figure 2) reveal that in the absence of Hg^{2+} the thymines in the T-rich loops are strongly reactive with OsO_4, whereas significant protection from reaction is seen in the presence of Hg^{2+} for most thymines that are predicted to form T-Hg^{2+}-T base pairs. This finding is consistent with the Hg^{2+}-dependent transition from a less structured state, where unpaired thymine residues are largely unstacked, to a rigidly stacked helical stem formed as a result of T-Hg^{2+}-T base pairing. Curiously, in all cases, no significant decrease in OsO_4 reactivity was observed for thymines within one nucleotide of the junction at the 3′-end of the Hg^{2+}-binding domain, despite the fact that the putative T-Hg^{2+}-T base pair partner at the 5′-end of the Hg^{2+}-binding domain showed significant protection from reactivity. Thus even though this base pair appears to form, one face of the OsO_4-reactive nucleotide remains unstacked and significantly exposed to solvent. Also notable was the decreased protection of a thymine near the junction in the conduction stem of the NB-1 and NB-2 constructs. These results are consistent with previous findings for natural three-way junction DNA, where it was observed that nucleobases near junctions that lack bulged nucleotides are unpaired and more reactive to OsO_4.[22] Such unstacking within a conductive stem in the Hg^{2+}-bound state foreshadows the Hg^{2+}-dependent inhibition of charge transport in the NB-1 construct (*vide infra*). In contrast, little change in the OsO_4 reactivity of conduction stem thymines was observed upon Hg^{2+} binding to any of the bulged junction constructs. This is again consistent with previous findings that bulged junctions can better accommodate the normal helical stacking of bases near the junction.[22] Overall, Hg^{2+} appears to bind as intended to induce helical stem formation in all of the Hg^{2+} binding domains being studied. However, the degree to which this structural change is able to bring about three-way junction charge transport switching remained to be tested.

Hg^{2+}-Fueled Switching of through-DNA Charge Transport. Charge transport switching in the Hg^{2+}-binding DNA constructs was investigated by examining the efficiency of electron−hole transport between the conductive helical stems. Specifically, photoexcitation of anthraquinone ("AQ", a photo-oxidant) leads to the injection of an electron−hole into the proximal, conductive helical stem to which the AQ is appended (Figure 1B).[24] The injected hole is then able to migrate from guanine to guanine within a stretch of well-stacked double-helix. We hypothesized that if sufficient nucleobase stacking were to occur at the three-way junction between the two conductive stems, efficient hole transport would occur between

dx.doi.org/10.1021/ja303530y | J. Am. Chem. Soc. 2012, 134, 13738−13748

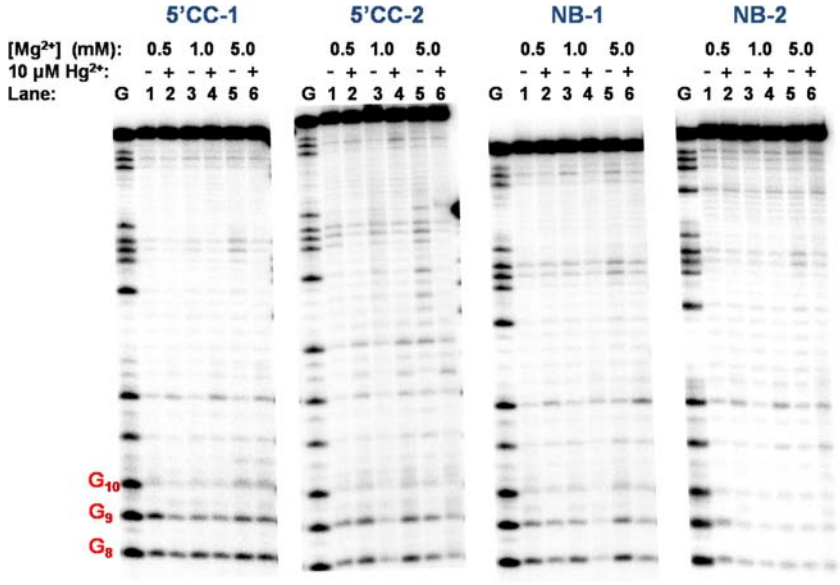

Figure 4. Survey of charge-flow-generated guanine damage patterns of different three-way junction switch constructs formed using the Hg^{2+}-binding domains shown in Figure 1C. Charge flow was assayed in the absence (-) and presence (+) of 10 μM Hg^{2+}, at three different Mg^{2+} concentrations (0.5, 1.0, and 5.0 mM). From left to right data are shown for 5′AA-1, 5′AA-2, 3′NB-1, and 3′NB-2. Lanes G show guanine sequencing ladders. Guanine triplets of interest (G_8-G_{10} and G_{24}-G_{26}), that are indicators of oxidative damage, are marked in red in correspondence to Figure 1.

them, leading to oxidative damage to specifically positioned "detector guanines" (G_8-G_{10} in Figure 1B). Such charge-flow-generated guanine oxidative damage is readily monitored by piperidine-induced DNA strand cleavage at the damage sites.[25] Light-irradiated AQ is capable of generating singlet oxygen ($^1O_2$), which has the ability to react directly with guanosine and give rise to DNA strand cleavage.[26] However, AQ remains a widely used hole injector into DNA because it has been multiply and rigorously tested that, under experimental conditions such as ours, $^1O_2$-generated guanine damage is not a significant problem.[27−29]

Hole transport efficiency was characterized for the eight DNA constructs shown in Figure 1B and 1C, at three different Mg^{2+} concentrations (0.5, 1, and 5 mM), and in the presence and absence of 10 μM Hg^{2+}. Figures 3 and 5 show that Hg^{2+}-dependent hole transport increase is observed, to varying degrees, in those constructs (3′AA-1, 3′AA-2, 3′CC-1, and 3′CC-2) that contain two bulged nucleotides where the 3′-end of the Hg^{2+}-binding domain meets the three-way junction. 3′AA-1 shows the most pronounced increase in hole transport efficiency, which varies little over the range of Mg^{2+} concentration tested. The 3′AA-2, 3′CC-1, and 3′CC-2 constructs, by contrast, show less dramatic hole transport switching, which is seen only at the higher Mg^{2+} concentrations. The observation of at least some Hg^{2+}-dependent increase in hole transport efficiency in all constructs that incorporate bulged nucleotides at the 3′-end of the Hg^{2+}-binding domain, is consistent with the lessons of earlier systematic studies on DNA three-way junction structure.[23] In such junctions, interhelical stacking is proposed to occur between two of the three helical stems, which in the present case, form the hole transport pathway.

Figures 4 and 5 show that Hg^{2+}-dependent hole transport switching is much more variable in constructs that either have no bulged nucleotides at the junction (NB-1 and NB-2), or have two bulged nucleotides at the 5′-attachment point of the Hg^{2+}-binding domain (5′CC-1 and 5′CC-2). Upon addition of

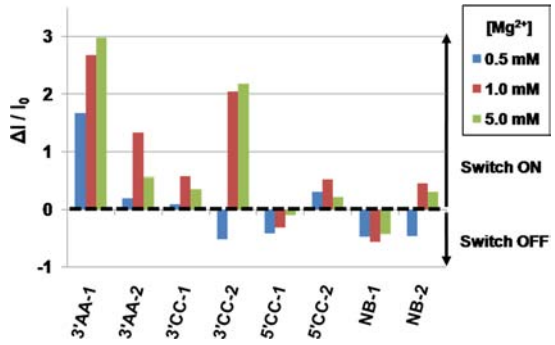

Figure 5. Quantification of the change in hole transport efficiency upon Hg^{2+} addition for each construct at each Mg^{2+} concentration for the data shown in Figures 3 and 4. $\Delta I/I_0$ represents the ratio of the change in $G_8 + G_9$ damage (as a percentage of all bands in a lane) at a given Hg^{2+} concentration (ΔI) to the $G_8 + G_9$ damage in the absence of Hg^{2+} (I_0). Typically, the error bars for charge transfer experiments are ~0.4 units of $\Delta I/I_0$ (see Figure 7).

Hg^{2+}, NB-2 shows either a small increase or decrease in hole transport efficiency, depending on the Mg^{2+} concentration. 5′CC-2 shows slight hole transport increase in the presence of Hg^{2+}, at all Mg^{2+} concentrations examined. Interestingly, the NB-1 construct (no bulged nucleotides at the junction), and to a lesser extent 5′CC-1, behave as *negative* hole transport switches, with their hole transport efficiency decreasing in response to Hg^{2+} binding. Fully base-paired three-way junctions without bulged nucleotides (such as NB-1 and NB-2 in their Hg^{2+}-bound states), are believed to adopt a symmetrical, trigonal conformation, which necessarily precludes coaxial interhelical stacking at the junction.[22] The switching data for NB-1 are wholly consistent with this. The OsO_4 footprinting data (Figure 2), too, are consistent with this finding, in that the conductive stem thymine residue at the junction is more solvent-exposed, and less stacked, in the Hg^{2+}-bound state (green arrow, Figure 2). Evidently, in the absence of Hg^{2+}, the

dx.doi.org/10.1021/ja303530y | J. Am. Chem. Soc. 2012, 134, 13738−13748

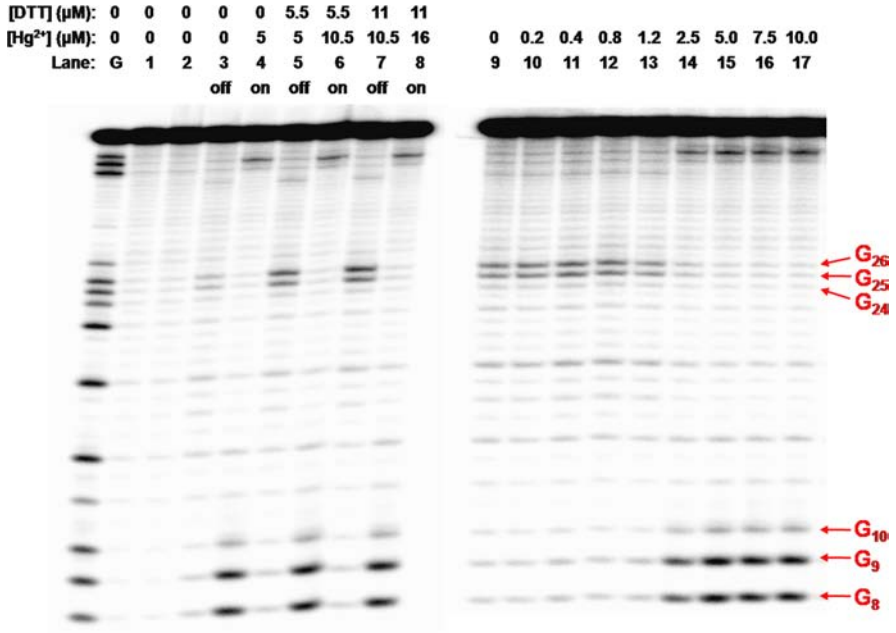

Figure 6. Electronic switching behavior of the 3′AA-1 DNA construct. Lane G shows a guanine sequence ladder. Lanes 1−17 show charge-flow-generated guanine damage patterns. Lanes 1 and 2 show negative controls where irradiation was omitted with an AQ-labeled 3′AA-1 (lane 1) and where 3′AA-1 lacking an AQ label was irradiated. Lanes 3−8 show the effect of alternating addition of Hg^{2+} and DTT. Lanes 9−17 show typical data for the dependence of DNA hole transport on $[Hg^{2+}]$. Guanine triplets of interest (G_8-G_{10} and G_{24}-G_{26}), that are indicators of oxidative damage, are marked in red in correspondence to Figure 1.

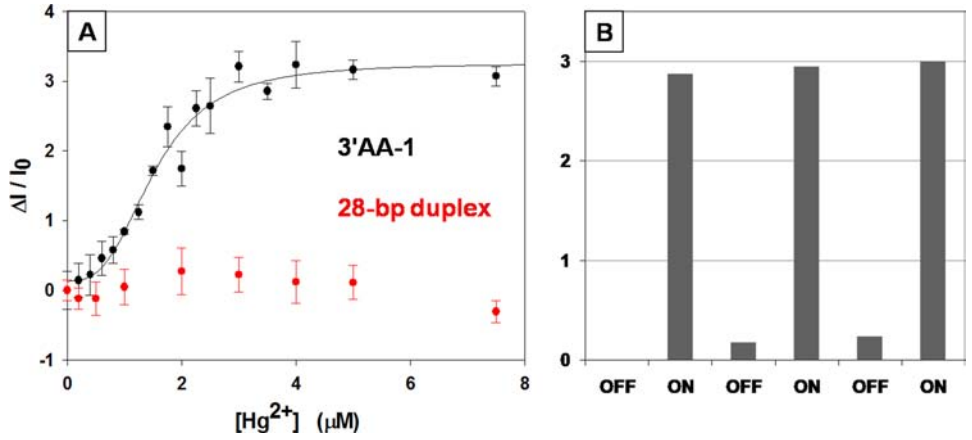

Figure 7. (A) Relative changes in charge-flow-induced DNA cleaved at G_8 and G_9 residues as functions of $[Hg^{2+}]$ for 3′AA-1 (black) and a 28-base pair duplex (red) with the same sequence as the helical hole transport path of 3′AA-1. $\Delta I/I_0$ represents the ratio of the change in $G_8 + G_9$ damage (as a percentage of all bands in a lane) at a given Hg^{2+} concentration (ΔI) to the $G_8 + G_9$ damage in the absence of Hg^{2+} (I_0). The 3′AA-1 data were fit to eq 1, which yielded an apparent K_d value of 1.52 ± 0.08 μM, and a Hill coefficient of 2.9 ± 0.4. Standard errors are plotted on the basis of three experimental replicates for 3′AA-1 and two replicates for the 28-base pair duplex. (B) Quantification of the change in $G_8 + G_9$ damage (as $\Delta I/I_0$) for repeated cycles of ON/OFF switching for 3′AA-1. The $G_8 + G_9$ damage for the initial OFF state was taken as I_0 for all subsequent ON/OFF cycles.

less structured nature of the mispaired Hg^{2+}-binding domain allows better stacking of the two conductive stems of NB-1, so that charge can flow between them.

As the 3′AA-1 construct demonstrates the most pronounced Hg^{2+}-dependent hole transport switching, we investigated its hole transport characteristics in greater detail. Figures 6 and 7B show that hole transport can be switched on and off, cleanly and repeatedly, by alternating additions and sequestrations (by DTT) of Hg^{2+}. Titration experiments (Figures 6, 7A and Supporting Information) show that Hg^{2+}-binding and the associated increase in hole transport efficiency are highly cooperative (Hill coefficient ∼3), as would be expected for duplex formation that depends on the closing of T-Hg^{2+}-T base pairs (quantification of $G_8 + G_9$ damage is described in the Materials and Methods section). Hole transport efficiency titration data were fit to eq 1, which yielded apparent affinity constant of 1.5 μM and a Hill coefficient of 2.9 (Figure 7A). Due to its cooperative response, 3′AA-1 shows a sharp change in hole transport efficiency over the 1−3 μM Hg^{2+} concentration range. By way of contrast, hole transport efficiency through a control duplex, with the same sequence as the putative hole transport path in 3′AA-1, is not significantly affected by the presence of Hg^{2+} and has a hole transport efficiency similar to that of 3′AA-1 in the latter's Hg^{2+}-bound state (Figure 7A, and Supporting Information). One curious observation from Figure 6 is that G_{25} and G_{26} of the G_{24}-G_{26}

dx.doi.org/10.1021/ja303530y | J. Am. Chem. Soc. 2012, 134, 13738−13748

guanine triplet located at the tip of the Hg^{2+}-binding loop show a modest susceptibility toward oxidative damage by the photoexcited AQ, but only in the Hg^{2+}-unbound state, where the loop's conformation is expected to be floppy. Upon Hg^{2+}-binding, this signal disappears, concomitant with high guanine damage and efficient hole transport to G_8/G_9 in the AQ-distal conduction stem. The observed G_{25}/G_{26} reactivity most likely does not arise from through-DNA hole transport from AQ, since both poorly structured DNA loops as well as T-T mismatches are known to block hole transport.[30] As described above, singlet oxygen-mediated guanine damage does not occur significantly under our experimental conditions. It is therefore likely, in consonance with an earlier observation by Santhosh and Schuster,[27] that damage to G_{25}/G_{26} is a result of direct, interstem contact of these bases (in the floppy, Hg^{2+}-unbound conformer of the three-way junction) with the AQ moiety. It is also theoretically possible that damage to G_{25}/G_{26} is a result of intermolecular contact with an AQ moiety, although such a possibility seems unlikely, given the very low concentrations of DNA in these experiments. The enhanced reactivity of the distal conduction stem guanines, G_8 and G_9, in the Hg^{2+}-bound state, however, necessarily results from through-DNA hole transport, as will be made clear from the fluorescence experiments described in the next section.

Mechanical Motion Associated with Charge Transport Switching. Having established that the 3′AA-1 constructs functions robustly as an electronic switch, we wished to investigate what kind of mechanical motion might be associated with hole transport switching. We therefore used Förster (fluorescence) resonance energy transfer experiments to probe for global conformational changes of the 3′AA-1 complex triggered by T-Hg^{2+}-T formation. For these experiments the cyanine fluorophores Cy3 and Cy5 were tethered (via C6-linkers) to the respective blunt-ended termini of the 3′AA-1 switch construct (Scheme 1). Such a dual-labeled construct

Scheme 1. FRET Measurements of Mechanical Motion Associated with Hg^{2+}-Fueled Hole Transport Switching in 3′AA-1

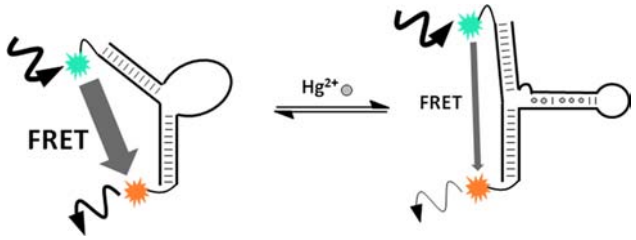

allowed the monitoring of Hg^{2+}-dependent movement of the conductive stems relative to one another, by measuring FRET efficiency (E_{FRET}) changes as Hg^{2+} was titrated into solution. This approach was modeled after the work of Lu and co-workers on metal cation-dependent 8-17 DNAzyme folding,[19] a system which superficially resembles our switch in that it involves the movement of helical stems about a bulged three-way junction. It should be noted that cyanine fluorophores appended through C3-linkers have been shown to stack upon the blunt ends of double stranded DNA,[20] a stacking that affects the value of the orientation factor κ and, in turn, the value of R_0.[21] Nevertheless, as shown by Lu and co-workers,[19] valuable quantitative information can be gleaned about folding transitions in such nucleic acid constructs using C6-linked cyanine fluorophores, as in the present case.

Figure 8A shows typical FRET spectra obtained for a Hg^{2+} titration experiment of Cy5/Cy3-labeled 3′AA-1. Clearly, Hg^{2+} addition leads to decreased acceptor emission and increased donor emission, which indicates decreased FRET energy transfer due to increased separation of the fluorophores. By contrast, control experiments performed with a Cy5-/Cy3-labeled 28-base pair duplex (same sequence as the switch conduction path) showed no significant change in emission spectra, and thus FRET efficiency, over the same Hg^{2+} concentration range investigated for 3′AA-1 (Figure 7B and Supporting Information). FRET efficiencies were calculated using the well described acceptor ratio, or "$(ratio)_A$", method,[18,19] which is a particularly appealing method because, as a ratiometric calculation, several potentially complicating factors such as dilution effects and acceptor quenching cancel out. In our experiments, Hg^{2+}-dependent donor quenching could complicate our interpretation by altering R_0 in a Hg^{2+}-dependent manner; however, we carried out control experiments with singly labeled (Cy3) 3′AA-1 and found that the donor emission was not affected significantly by the presence of Hg^{2+} over the relevant concentration range (see Supporting Information). Figure 8B plots FRET efficiency (calculated using eq 2, Materials and Methods) as a function of Hg^{2+} concentration for both the dual-labeled 3′AA-1 and the dual-labeled 28-base pair duplex. The FRET efficiency data from Figure 8B were converted to average Cy3-Cy5 distances (shown in Figure 8C) using eq 4 (Materials and Methods). The Hg^{2+} concentration dependence of both the FRET efficiency and interfluorophore distance were fitted to cooperative binding isotherms, as had been done, above, for the hole transport switching data (see eqs 1 and 3, Materials and Methods). For the 28-base pair control duplex, the FRET data provide an average interfluorophore distance estimate of 98.8 ± 0.1 Å, which is credible in terms of their expected separation assuming the typical base pair rise distance of 3.4 Å,[31] in a rigid 28-base pair duplex (95.2 Å). Our FRET data thus provide perfectly reasonable distance data, irrespective of whether the C6-linked fluorophores are mobile in space about the helix termini, or stacked upon the ends of the DNA helix.

On the basis of comparison of the FRET and hole transport switching data (Figure 8C), the mechanical response of 3′AA-1 appears to be strongly correlated with the change in hole transport efficiency across the three-way junction. Compared to the hole transport switching data, a slightly lower apparent Hg^{2+} binding constant (0.83 μM and 1.14 μM from fitting the FRET efficiency and interfluorophore distance data, respectively, compared to 1.52 μM obtained for hole transport switching) and lower apparent cooperativity (Hill coefficient of ~2, as opposed to ~3 for hole transport switching) was observed for the mechanical response of 3′AA-1. These relatively modest discrepancies no doubt reflect the very different physical bases for the two readouts. The greater apparent cooperativity and lower apparent Hg^{2+}-binding constant for hole transport switching is consistent with a model in which full occupancy of the multiple Hg^{2+}-binding sites (T-Hg^{2+}-T base pairs) is required to bring about productive stacking and electrical contact between the conductive stems. On the other hand, mechanical motion appears to commence before full occupancy of the available Hg^{2+}-binding sites has been achieved. These minor differences notwithstanding, the data for 3′AA-1 demonstrate overall the

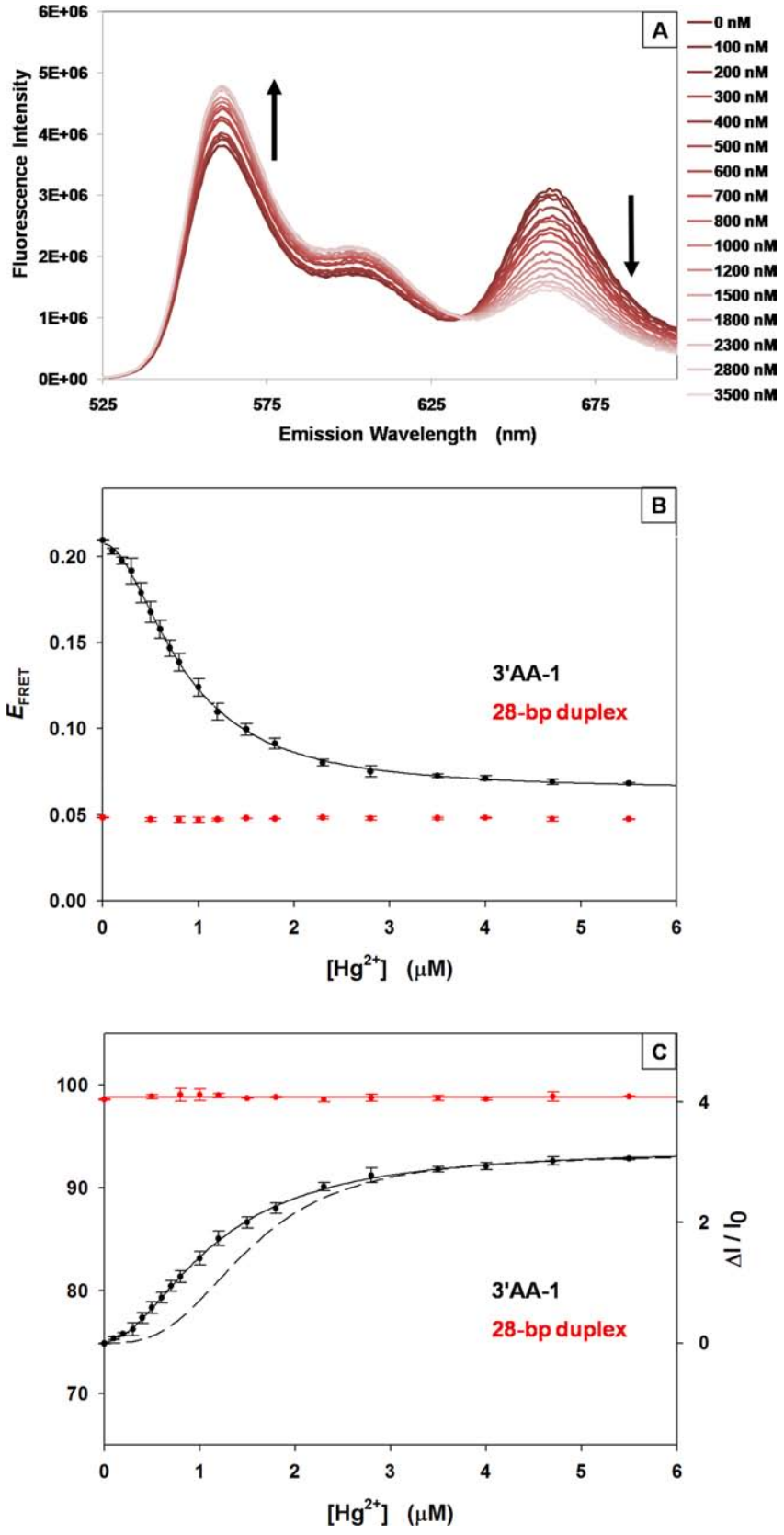

Figure 8. (A) FRET emission spectra (λ_{ex}^{D} = 513 nm) obtained from Hg^{2+} titration of 3′AA-1 labeled with Cy3 and Cy5 at its respective 5′-termini. Binding of Hg^{2+} to 3′AA-1 causes increased donor emission and decreased acceptor emission, which indicates decreased FRET efficiency. FRET spectra for the 28-base pair duplex control did not change significantly upon similar titration with Hg^{2+} (see Supporting Information). (B) Plot of FRET efficiency as a function of $[Hg^{2+}]$ for 3′AA-1 (black); and a 28-base pair duplex with the same sequence as the conductive helical stems of 3′AA-1. 3′AA-1 data were fit to eq 3, which yielded an apparent binding constant of 0.83 ± 0.02 μM, and a Hill coefficient of 1.92 ± 0.07. (C) Plot of average interfluorophore distances calculated from E_{FRET} values using eq 4. Data were fit to a cooperative binding isotherm (eq 1), which yielded an

dx.doi.org/10.1021/ja303530y | J. Am. Chem. Soc. 2012, 134, 13738−13748

Figure 8. continued

apparent binding constant of 1.14 ± 0.03 μM, and a Hill coefficient of 1.89 ± 0.07. The fitted interfluorophore distances in the absence of Hg^{2+} and at Hg^{2+} saturation were 75.0 ± 0.2 nm and 93.8 ± 0.5 nm, respectively. The average interfluorophore distance for the 28-base pair duplex was 98.8 ± 0.1 nm. In panel (C), the Hg^{2+} binding curve obtained from fitting the hole transport switching data in Figure 7A is plotted (dashed line) alongside the binding curve obtained from FRET, for comparison . Standard errors in E_{FRET} and average interfluorophore distance values are plotted on the basis of three experimental replicates for 3′AA-1 and two replicates for the 28-base pair sample.

hole transport efficiency switching is indeed tightly coupled with mechanical motion of the conductive stems relative to one another.

The FRET data also help to shed light on the mechanism underlying the switch in hole transport efficiency across the three-way junction. As shown in Figure 8C, in the Hg^{2+}-saturated state, the average interfluorophore distance for 3′AA-1 approaches to within ∼5 Å of that of the comparable 28-base pair duplex (the fitted 3′AA-1 average interfluorophore distance at Hg^{2+}-saturation was 93.8 Å vs 98.8 Å for the 28-base pair duplex). Given the close correspondence of the Hg^{2+}-dependences of the FRET and hole transport responses, the interfluorophore distance data clearly demonstrate that efficient hole transport coincides with the formation of a structure closer to one in which the conductive stems adopt a stacked, nearly colinear geometry. On the basis of the interfluorophore distance data shown in Figure 8C and the assumption that 14-base pair stems are rigid with junction-to-fluorophore lengths of 49.4 Å, simple geometrical calculations show that the observed change in average interfluorophore distance of ∼19 Å corresponds to a change in the average angle between the conductive stems from ∼101° to ∼143° upon full Hg^{2+} binding. However, these data do not speak to the flexibility of 3′AA-1; it is possible that 3′AA-1 only transiently adopts a fully stacked junction conformation, in which the angle between the conductive stems is closer to 180°. This type of mechanistic model would be consistent with the average junction angle of <180° observed for 3′AA-1 and with the well-known flexibility observed in natural three-way junctions.[32]

The fact that the average distance between the termini of the conductive stems increases with Hg^{2+} binding rules out direct AQ contact with the detector guanines (G_8-G_{10}) as the mechanism of Hg^{2+}-dependent hole transport, and confirms that AQ remotely oxidizes G_8-G_{10} by a through-DNA hole transport process, necessarily depending upon electrical contact at the three-way junction. It also removes any lingering possibility that diffusible reactive oxygen species, such as $^1O_2$, produced during irradiation of the AQ moiety, may be involved in the enhanced reactivity of the detector guanines, G_8-G_{10}, seen in the 'on' conformer, relative to the 'off' conformer. The FRET data show unequivocally that in the 'on' conformer these guanines are further away from the AQ moiety than in the 'off' conformer, rendering moot any putative role of diffusible oxygen species. Overall, then, the FRET data demonstrate that hole transport switching in 3′AA-1 is associated with a significant change in junction geometry, from a bent toward a more linear arrangement of the conductive stems upon Hg^{2+} binding.

CONCLUSIONS

We have described a three-way junction-based, multiply reversible DNA switch that responds in a cooperative fashion to Hg^{2+} binding. Our data demonstrate that Hg^{2+} binding induces a 'closed' conformation in which charge transport increases across the junction separating two conductive helical stems. FRET experiments show that this switching of junction electron−hole transport efficiency results from changes in the relative orientations of the conductive stems about the junction. Specifically, the nonconductive 'open' state corresponds to a bent relationship between the conductive stems, whereas in the 'closed' state, the conductive stems move toward a more linear arrangement, such that interhelical stacking can occur so as to permit charge flow. Thus, our DNA switch provides a unique example of a DNA nanomachine in which mechanical motion is tightly coupled to, and causal of, changes in hole transport efficiency. While our system serves as a basic proof of this principle, this type of mechano-electronic switching may provide for electrical monitoring of structural responses in DNA nanoscience and nanofabrications. Efforts are now under way to reconstitute the current Hg^{2+}-triggered switch in a redox-labeled, electrode-bound format, to provide a simple analytical sensor for Hg^{2+} with an electrical readout, as has been accomplished with three-way junction-based sensors for other analytes.[12]

ASSOCIATED CONTENT

Supporting Information

Supplementary charge transport and fluorescence data. This material is available free of charge via the Internet at http://pubs.acs.org.

AUTHOR INFORMATION

Corresponding Author

sen@sfu.ca; hzyu@sfu.ca

Notes

The authors declare no competing financial interest.

ACKNOWLEDGMENTS

We thank Edgar Young for his insights into FRET methods and analysis. This work was supported by grants from the Natural Sciences and Engineering Research Council of Canada (NSERC) to H.-Z.Y. and to D.S.; and by a Collaborative Health Research Project (CHRP) Grant from NSERC and the Canadian Institutes for Health Research (CIHR) to H.-Z.Y. and D.S. D.S. is a fellow of the Canadian Institute for Advanced Research (CIFAR).

REFERENCES

(1) (a) Seeman, N. C. *Trends Biochem. Sci.* **2005**, *30*, 119−125. (b) Bath, J.; Turberfield, A. J. *Nat. Nanotechnol.* **2007**, *2*, 275−284. (c) Seeman, N. C. *Annu. Rev. Biochem.* **2010**, *79*, 65−87. (d) Teller, C.; Wilner, I. *Curr. Opin. Biotechnol.* **2010**, *21*, 376−391. (e) Krishnan, Y.; Simmel, F. C. *Angew. Chem.* **2011**, *50*, 3124−3156.

(2) Chen, Y.; Lee, S.-H.; Mao, C. *Angew. Chem.* **2004**, *43*, 5335−5338.

(3) Modi, S.; Swetha, M. G.; Goswami, D.; Gupta, G. D.; Mayor, S.; Krishnan, Y. *Nat. Nanotechnol.* **2009**, *4*, 325−330.

(4) (a) Alberti, P.; Mergny, J.-L. *Proc. Natl. Acad. Sci. U.S.A.* **2003**, *100*, 1569−1573. (b) Hou, X.; Guo, W.; Xia, F.; Nie, F.-Q.; Dong, H.; Tian, Y.; Wen, L.; Wang, L.; Cao, L.; Yang, Y.; Xue, J.; Song, Y.; Wang, Y.; Liu, D.; Jiang, L. *J. Am. Chem. Soc.* **2009**, *131*, 7800−7805.
(5) Mao, C.; Sun, W.; Shen, Z.; Seeman, N. C. *Nature* **1999**, *397*, 144−146.
(6) (a) Yurke, B.; Turberfield, A. J.; Mills, A. P.; Simmel, F. C.; Neumann, J. L. *Nature* **2000**, *406*, 605−608. (b) Zhang, D. Y.; Seelig, G. *Nature Chem.* **2011**, *3*, 103−113.
(7) (a) Yan, H.; Zhang, X.; Shen, Z.; Seeman, N. C. *Nature* **2002**, *415*, 62−65. (b) Chen, Y.; Wang, M.; Mao, C. *Angew. Chem.* **2004**, *43*, 3554−3557. (c) Chen, Y.; Mao, C. *J. Am. Chem. Soc.* **2004**, *126*, 8626−8627. (d) Muscat, R. A.; Bath, J.; Turberfield, A. J. *Nano Lett.* **2011**, *11*, 982−987.
(8) (a) Shin, J.-S.; Pierce, N. A. *J. Am. Chem. Soc.* **2004**, *126*, 10834−10835. (b) Sherman, W. B.; Seeman, N. C. *Nano Lett.* **2004**, *4*, 1203−1207. (c) Omabegho, T.; Sha, R.; Seeman, N. C. *Science* **2009**, *324*, 67−71.
(9) (a) Hu, Y.; Liu, D. R. *Nat. Nanotechnol.* **2010**, *5*, 778−782. (b) Lund, K.; Manzo, A. J.; Dabby, N.; Michelotti, N.; Johnson-Buck, A.; Nangreave, J.; Taylor, S.; Pei, R.; Stojanovic, M. N.; Walter, N. G.; Winfree, E.; Yan, H. *Nature* **2010**, *465*, 206−210.
(10) You, M.; Chen, Y.; Zhang, X.; Liu, H.; Wang, R.; Wang, K.; Williams, K. R.; Tan, W. *Angew. Chem.* **2012**, *51*, 2457−2460.
(11) Buranachai, C.; McKinney, S. A.; Ha, T. *Nano Lett.* **2006**, *6*, 496−500.
(12) (a) Fahlman, R. P.; Sen, D. *J. Am. Chem. Soc.* **2002**, *124*, 4610−4616. (b) Sankar, C. G.; Sen, D. *J. Mol. Biol.* **2004**, *340*, 459−467. (c) Huang, Y. C.; Ge, B.; Sen, D.; Yu, H.-Z. *J. Am. Chem. Soc.* **2008**, *130*, 8023−8029.
(13) Seemann, I. T.; Singh, V.; Azarkh, M.; Drescher, M.; Hartig, J. S. *J. Am. Chem. Soc.* **2011**, *133*, 4706−4709.
(14) Huang, Y. C.; Sen, D. *J. Am. Chem. Soc.* **2010**, *132*, 2663−2671. (b) Ge, B.; Huang, Y. C.; Sen, D.; Yu, H.-Z. *Angew. Chem.* **2010**, *49*, 9965−9967.
(15) Ono, A.; Torigoe, H.; Tanaka, Y.; Okamoto, I. *Chem. Soc. Rev.* **2011**, *40*, 5855−5866.
(16) (a) Ono, A.; Togashi, H. *Angew. Chem.* **2004**, *43*, 4300−4302. (b) Zhang, X.-B.; Kong, R.-M.; Lu, Y. *Annu. Rev. Anal. Chem.* **2011**, *4*, 105−128.
(17) Telser, J.; Cruickshank, K. A.; Morrison, L. E.; Netzel, T. L.; Chan, K. *J. Am. Chem. Soc.* **1989**, *111*, 7226−7232.
(18) Clegg, R. M. *Methods Enzymol.* **1992**, *211*, 353−388.
(19) (a) Kim, H.-K.; Liu, J.; Li, J.; Nagraj, N.; Li, M.; Pavot, C.M.-B.; Lu, Y. *J. Am. Chem. Soc.* **2007**, *129*, 6896−6902. (b) Mazumdar, D.; Nagraj, N.; Kim, H.-K.; Meng, X.; Brown, A. K.; Sun, Q.; Li, W.; Lu, Y. *J. Am. Chem. Soc.* **2009**, *131*, 5506−5515.
(20) (a) Norman, D. G.; Grainger, R. J.; Uhrin, D.; Lilley, D. M. J. *Biochemistry* **2000**, *39*, 6317−6324. (b) Iqbal, A.; Wang, L.; Thompson, K. C.; Lilley, D. M. J.; Norman, D. G. *Biochemistry* **2008**, *47*, 7857−7862.
(21) Iqbal, A.; Arslan, S.; Okumus, B.; Wilson, T. J.; Giraud, G.; Norman, D. G.; Ha, T.; Lilley, D. M. J. *Proc. Natl. Acad. Sci. U.S.A.* **2008**, *105*, 11176−11181.
(22) Duckett, D. R.; Lilley, D. M. J. *EMBO J.* **1990**, *9*, 1659−1664.
(23) (a) Welch, J. B.; Duckett, D. R.; Lilley., D. M. J. *Nucleic Acids Res.* **1993**, *21*, 4548−4555. (b) Rosen, M. A.; Patel, D. J. *Biochemistry* **1993**, *32*, 6576−6587. (c) Leontis, N. B.; Hills, M. T.; Piotto, M.; Ouporov, I. V.; Malhotra, A.; Gorenstein, D. G. *Biophys. J.* **1995**, *68*, 251−265. (d) Overmars, F. J.; Pikkemaat, J. A.; van den Elst, H.; van Boom, J. H.; Altona, C. *J. Mol. Biol.* **1996**, *255*, 702−713. (e) Stuhmeier, F.; Welch, J. B.; Murchie, A. I.; Lilley, D. M. J.; Clegg, R. M. *Biochemistry* **1997**, *36*, 13530−13538. (f) Lilley, D. M. J. *Q. Rev. Biophys.* **2000**, *33*, 109−159.
(24) Gasper, S. M.; Schuster, G. B. *J. Am. Chem. Soc.* **1997**, *119*, 12762−12771.
(25) Hall, D. B.; Holmlin, R. E.; Barton, J. K. *Nature* **1996**, *382*, 731−735.
(26) Devasagayam, T. P.; Steenken, S.; Obendorf, M. S.; Schulz, W. A.; Sies, H. *Biochemistry* **1991**, *30*, 6283−6289.
(27) Santhosh, U.; Schuster, G. B. *Nucleic Acids Res.* **2003**, *31*, 5692−5699.
(28) P.T. Henderson, P. T.; Jones, D.; Hampikian, G.; Kan, Y.; Schuster, G. B. *Proc. Natl. Acad. Sci. U.S.A.* **1999**, *96*, 8353−8358.
(29) Leung, E. K. Y.; Sen, D. *Chem .Biol.* **2007**, *14*, 41−51.
(30) Joseph, J.; Schuster, G. B. *J. Am. Chem. Soc.* **2009**, *131*, 13904−13905.
(31) Voet, D.; Voet, J. G. *Biochemistry*; John Wiley & Sons: New York, 1995.
(32) (a) Ma, R. I.; Kallenbach, N. R.; Sheardy, R. D.; Petrillo, M. L.; Seeman, N. C. *Nucleic Acids Res.* **1986**, *14*, 9745−9753. (b) Yang, M.; Millar, D. P. *Biochemistry* **1996**, *35*, 7959−7967. (c) Shlyakhtenko, L. S.; Potaman, V. N.; Sinden, R. R.; Gall, A. A.; Lyubchenko, Y. L. *Nucleic Acids Res.* **2000**, *28*, 3472−3477.